VNUHCM Journal of Science and Technology Development 2026, 29(2):4083-4089

Open Access Full Text Article

Research article

Plasmon properties in monolayer silicene: Effects of temperature

Dong Thi Kim Phuong[1,2], Nguyen Van Men[1,2,*]

Use your smartphone to scan this QR code and download this article

ABSTRACT

This paper presents a theoretical investigation of the plasmon excitation spectrum in monolayer silicene systems at finite temperatures under the random-phase approximation. Because of silicene's buckled honeycomb structure and strong spin–orbit coupling ($\triangle_{so}$), its bandgap can be tuned electrically via an external perpendicular field that induces a sublattice potential difference ($\triangle_z$). This study examines how temperature and $\triangle_z$ influence plasmon dispersion, damping, and stability. The results show that the plasmon mode maintains its characteristic $\sqrt{q}$ dependence on the wave vector at long wavelengths but undergoes a pronounced redshift and enhanced Landau damping as the temperature increases, particularly near the critical condition $\triangle_z \approx \triangle_{so}$, where the electronic gap closes and the single-particle excitation region expands. When the gap reopens, the undamped plasmon region is restored, and the mode becomes more stable. Moreover, the plasmon frequency depends nonmonotonically on temperature, decreasing at intermediate temperatures and increasing again at higher values as a result of thermal carrier activation. These findings demonstrate the importance of thermal and electric-field effects in determining the plasmonic behavior of silicene and could inform the design of stable, tunable plasmonic and optoelectronic devices based on two-dimensional silicon.

Key words: Finite temperature effects, Monolayer silicene, Plasmon excitation, Random phase approximation, Spin–orbit coupling, Sublattice asymmetry

[1]*An Giang University, Viet Nam National University Ho Chi Minh City, An Giang province, Vietnam*

[2]*Viet Nam National University Ho Chi Minh City, Ho Chi Minh City, Vietnam*

Correspondence

Nguyen Van Men, An Giang University, Viet Nam National University Ho Chi Minh City, An Giang province, Vietnam

Viet Nam National University Ho Chi Minh City, Ho Chi Minh City, Vietnam

Email: nvmen@agu.edu.vn

History

- Received: 13-10-2025
- Revised: 18-01-2026
- Accepted: 23-02-2026
- Published Online: 11-06-2026

DOI : 10.32508/vnuhcmj-std.v29i2.4623

Check for updates

INTRODUCTION

Two-dimensional (2D) materials have become a major focus of condensed matter research because of their remarkable electronic, optical, and mechanical properties. Following the isolation of graphene, a wide range of 2D materials has been synthesized and studied, including silicene, germanene, and transition-metal dichalcogenides[1,2]. Silicene, a monolayer of silicon atoms arranged in a honeycomb lattice, has attracted significant attention owing to its compatibility with current silicon-based semiconductor technology and its unique buckled atomic configuration. The buckling arises from mixed sp^2-sp^3 hybridization and enables the electronic band structure of silicene to be tuned effectively by a perpendicular electric field. This structural and electronic versatility makes silicene a promising material for next-generation nanoelectronic and plasmonic devices[3–5]. In electron systems, plasmons are collective oscillations of the charge density and are a key manifestation of many-body effects. The plasmon dispersion of a material provides information about its dielectric response, screening effects, and carrier dynamics. In recent years, 2D plasmons have been extensively investigated because of their potential applications in plasmonic waveguides, optical modulators, terahertz detectors, and nanoscale photonic circuits. The prospect of confining and manipulating electromagnetic energy beyond the diffraction limit has stimulated widespread interest in integrating plasmonic functionalities into 2D materials[6–10].

Early studies on graphene established the foundation of 2D plasmonics by showing that plasmon modes can be tuned efficiently by adjusting the carrier density, gate voltage, or substrate environment[6,11–13]. Silicene, however, differs from graphene in several key aspects: it has a finite bandgap that can be controlled by an external electric field and exhibits significant spin–orbit coupling. These features give rise to rich electronic phases, including topological insulating and spin-valley polarized metallic states, each characterized by distinct collective excitation spectra. Theoretical analyses by Tabert and Nicol[3], Pyatkovskiy[14], and others have demonstrated that the plasmon modes in monolayer silicene (MLS) can be tuned by varying the external field strength or chemical potential. Experimentally, plasmon resonances in silicene have been observed in the terahertz and near-infrared regimes, indicating potential applications in high-speed optoelectronic and sensing technologies[2,5,15–17].

Despite these advances, most investigations have been restricted to zero-temperature ($T = 0K$) conditions,

Cite this article : Thi Kim Phuong D, Van Men N. **Plasmon properties in monolayer silicene: Effects of temperature**. *VNUHCM J. Sci. Technol. Dev.* 2026; 29(2):4083-4089.

in which thermal effects are neglected. In realistic environments, thermal broadening of the Fermi–Dirac distribution modifies the dielectric response and the plasmon characteristics [3,5,18–20]. Specifically, a finite temperature introduces additional damping mechanisms through intra- and interband excitations, which can shift the plasmon dispersion and reduce its lifetime. A full understanding of these thermal effects is needed for accurate modeling of plasmonic excitations and predicting device performance under practical conditions.

In this work, we investigate the plasmon modes in MLS at finite temperature using the random-phase approximation (RPA). We calculate the dielectric function and analyze the temperature dependence of plasmon dispersion and damping under various external parameter values. The findings yield information about the thermally induced evolution of plasmonic behavior in silicene and provide a theoretical basis for the development of 2D plasmonic and optoelectronic devices that can operate at room temperature. Although finite-temperature collective excitations in silicene have been investigated previously, most existing studies focused on fixed bandgaps. In contrast, the present work systematically explores the combined effects of temperature and electrically tunable sublattice asymmetry across the entire gap closing and reopening transition, focusing on the critical condition $\triangle_z \approx \triangle_{so}$ [3,17,21].

THEORETICAL APPROACH

Previous studies have shown that the polarization function of MLS at wave vector q, frequency ω, and temperature T is given by the following (3):

$$\Pi^0(q,\omega,T) = \frac{1}{8\pi^2}\sum_{\sigma,\xi=\pm1}\int d^2\overrightarrow{k}\sum_{\lambda,\lambda'=\pm}$$

$$\left\{\left(1+\lambda\lambda'\frac{h^2v_F^2k\left(\overrightarrow{q}+\overrightarrow{k}\right)+\triangle_{\sigma\xi}^2}{E_{\sigma\xi}\left(\overrightarrow{k}\right)E_{\sigma\xi}\left(\overrightarrow{k}+\overrightarrow{q}\right)}\right)\right.$$

$$\left.\times\frac{n_F\left[\lambda E_{\sigma\xi}\left(\overrightarrow{k}\right)\right]-n_F\left[\lambda' E_{\sigma\xi}\left(\overrightarrow{k}+\overrightarrow{q}\right)\right]}{\lambda E_{\sigma\xi}\left(\overrightarrow{k}\right)-\lambda' E_{\sigma\xi}\left(\overrightarrow{k}+\overrightarrow{q}\right)-\omega-i0^+}\right\} \quad (1)$$

Where

$$E_{\sigma\xi}\left(\overrightarrow{k}\right) = \lambda\sqrt{h^2v_F^2\overrightarrow{k}^2+\triangle_{\sigma\xi}^2} \quad (2)$$

denotes the Fermi energy of electrons in MLS ($\sigma = \pm1$ and $\xi = \pm1$ correspond the spin and valley indices, respectively; $\lambda = \pm1$ denotes conduction or valence bands), and

$$n_F(E) = \left[exp\left(\frac{E-\mu}{k_BT}\right)+1\right]^{-1} \quad (3)$$

is the Fermi-Dirac distribution function, and μ is the chemical potential, which equals the Fermi energy at zero temperature.

The chemical potential μ is determined as the solution of the following equation [22]:

$$\left(\frac{hv_F}{k_BT}\right)^2 n = \sum_{\gamma=\pm1}\frac{\gamma}{\pi}\sum_{i=<,>}$$

$$\left\{-Li_2\left[-exp\left(\frac{\gamma\mu(T)-\triangle_i}{k_BT}\right)\right]\right.$$

$$\left.+\frac{\triangle_i}{k_BT}\ln\left[1+exp\left(\frac{\gamma\mu(T)-\triangle_i}{k_BT}\right)\right]\right\} \quad (4)$$

With

$$\triangle_< = |\triangle_{so}-\triangle_z|,\ \triangle_> = \triangle_{so}+\triangle_z \text{ and } (5)$$

$$Li_2(z) = -\int_0^z\frac{\ln(1-t)}{t}dt \quad (6)$$

Within the RPA, the dielectric function is expressed as [3,20–27]:

$$\varepsilon = 1 - v(q)\Pi^0(q,\omega,T) \quad (7)$$

In which

$$v(\overrightarrow{q}) = \frac{2\pi\alpha}{q} \quad (8)$$

$$\alpha = \frac{e^2}{4\pi\varepsilon_0\kappa}\ (\kappa \textit{ is the permitivity of the substrate}). \quad (9)$$

The plasmon spectrum of the system can be determined from the zero-point condition of the temperature-dependent dynamical dielectric function [25,28–32].

$$\varepsilon\left(q,\omega_p-i\gamma,T\right) = 0 \quad (10)$$

In equation (10), ω_p represents the plasmon frequency corresponding to the wave vector q, while γ denotes the damping coefficient associated with the plasma oscillations. In the weak-damping limit, the plasmon spectrum can be approximately determined from the zero condition of the real part of the dielectric function [25,28–32].

$$Re\varepsilon\left(q,\omega_p,T\right) = 0. \quad (11)$$

The numerical solutions of this equation, obtained using the dielectric function given by equation (7) and the polarization function defined in equation (1), yield the plasmon excitation spectrum of the system. The present analysis is performed within the RPA, which neglects exchange–correlation and vertex corrections. Although the RPA provides a reliable description of collective excitations in doped Dirac systems, such beyond-RPA effects may become increasingly relevant at high temperatures. Therefore, the high-temperature results should be interpreted primarily in a qualitative sense [3,17,21,32].

RESULTS AND DISCUSSION

In this section, we present the numerical results for the collective excitation spectrum in MLS systems, taking into account the effects of finite temperature. The symbols E_F, k_F *and* T_F denote, respectively, the Fermi energy, Fermi wave vector, and Fermi temperature of the MLS system.

Figure 1 shows the plasmon dispersion of MLS at various reduced temperatures with fixed parameters

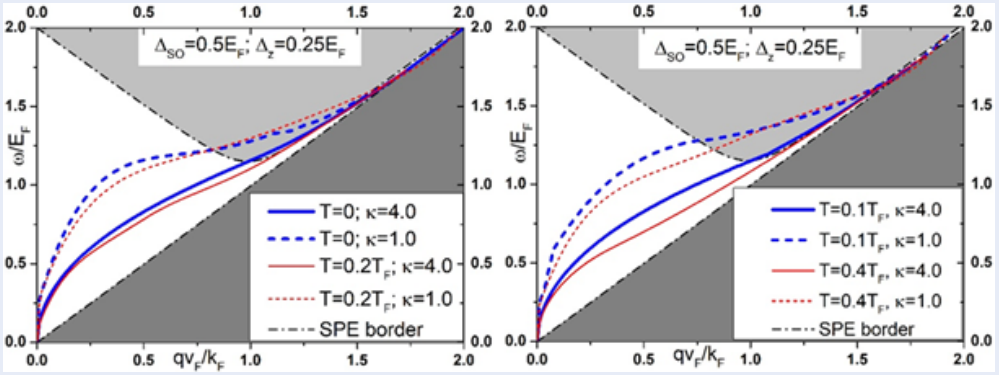

Figure 1: Temperature-dependentplasmon dispersion in monolayer silicene (MLS) at $\triangle_{so} = 0.5\ E_F$ *and* $\triangle_z = 0.25\ E_F$. Curvescorrespond to increasing temperatures $T = 0$, $T = 0.1T_F$, $T = 0.2T_F$ *and* $T = 0.4T_F$. Theshaded regions denote the SPE continua at zero temperature.

$\triangle_{so} = 0.5\ E_F$ *and* $\triangle_z = 0.25\ E_F$. The solid curves represent the plasmon modes, whereas the shaded regions indicate the single-particle excitation (SPE) continua at zero temperature. In the long-wavelength limit, the dispersion exhibits the characteristic $\sqrt{q}$ dependence of two-dimensional collective charge oscillations.

At zero temperature ($T = 0$), the plasmon branch lies completely outside the intraband SPE region, implying negligible Landau damping and a well-defined collective mode. When the temperature increases ($T = 0$, $T = 0.1T_F$, $T = 0.2T_F$ *and* $T = 0.4T_F$), the plasmon frequency decreases slightly, and the dispersion curves shift downward. This redshift originates from the thermal broadening of the Fermi–Dirac distribution, which effectively reduces the number of carriers contributing to collective oscillations. Simultaneously, the overlap between the plasmon branch and the SPE region increases, leading to enhanced damping and a shorter plasmon lifetime. Similar behaviors have been found in the plasmon properties of graphene and graphene-based systems[23,25,33,34].

Comparing the two panels of Figure 1 reveals that thermal effects become more pronounced at higher temperatures. At $T = 0$, $T = 0.1T_F$, $T = 0.2T_F$ *and* $T = 0.4T_F$, the low-energy plasmon branch partially enters the SPE continuum, signaling the onset of strong damping. Nevertheless, the mode remains discernible, indicating that collective excitations in silicene are robust up to moderate thermal energies. These results demonstrate the importance of finite-temperature effects in determining the plasmonic response of MLS and provide theoretical guidance for designing silicene-based plasmonic devices operating near room temperature.

To assess the role of environmental screening, we explicitly include the vacuum limit ($\kappa = 1.0$) in [1], which isolates the intrinsic plasmonic response of MLS. Although the absolute plasmon frequencies are rescaled by the effective dielectric constant κ, the temperature-induced redshift, damping behavior, and gap-closure effects are largely unchanged. This confirms that the main conclusions of this work are robust against substrate screening and are not specific to a particular dielectric environment[3,20].

Figure 2 shows the plasmon dispersion of MLS at two reduced temperatures ($T = 0$, $T = 0.1T_F$, $T = 0.2T_F$ *and* $T = 0.4T_F$) for four perpendicular-field-induced sublattice asymmetries $\triangle_z$. Increasing the temperature produces a systematic redshift and brings the mode closer to the SPE boundary, consistent with thermal broadening of the Fermi–Dirac distribution and enhanced Landau damping. Varying $\triangle_z$ reorganizes the interband threshold and, consequently, the undamped window. For $\triangle_z = 0$ (the upper left panel), the gap is determined solely by spin–orbit coupling; the interband SPE edge sits relatively high, so the plasmon remains outside the continuum over a wide range of q values, with modest temperature sensitivity. At $\triangle_z = 0.2E_F$ (the upper right panel), the reduced gap for one spin/valley lowers the interband threshold, slightly narrowing the undamped window and increasing damping at intermediate q. The most pronounced change occurs at $\triangle_z = 0.3E_F$ (the lower right panel), where one gap associated with a mass term closes ($|\triangle_{so} - \triangle_z = 0|$). The interband threshold collapses, the SPE continuum expands toward low energy, and the plasmon intersects the continuum at smaller q, making the temperature-induced redshift and damping more visible. For $\triangle_z = 0.4E_F$ (the lower

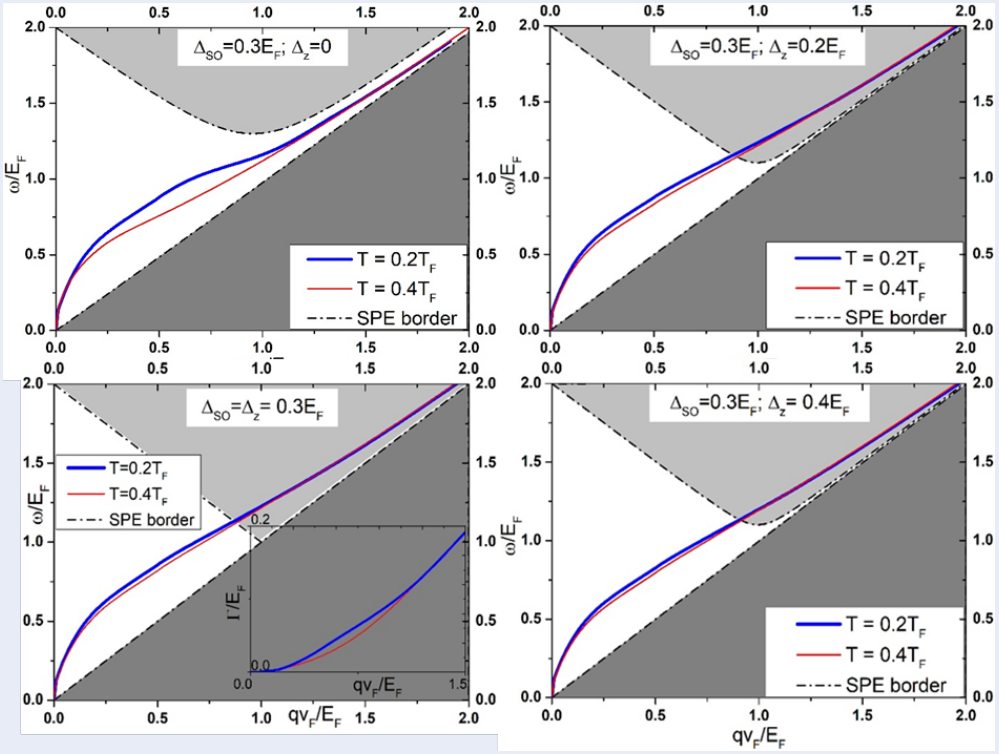

Figure 2: Plasmon modes in MLS at $T = 0$, $T = 0.1T_F$, $T = 0.2T_F$ *and* $T = 0.4T_F$, plotted for $\triangle_z = 0.3E_F$ and several $\triangle_z$ values. The inset in thelower left panel denotes the corresponding broadening function. The shade-dregions denote the SPE continua at zero temperature.

right panel), the gap reopens ($|\triangle_{so} - \triangle_z = 0|$), and the interband boundary shifts upward again, partially restoring the undamped region and reducing thermal sensitivity relative to the previous case. Overall, $\triangle_z$ acts as a tunable control of the plasmon damping landscape: the undamped window is largest away from the gap-closure point and smallest near $\triangle_z \approx \triangle_{so}$. These trends indicate that at a high temperature, devices would benefit from operating in regimes with reopened gaps ($\triangle_z \neq \triangle_{so}$), where plasmon modes remain sharper over a broader momentum range.

The inset in the lower left panel of Figure 2 shows the broadening function Γ associated with the plasmon mode. This quantity originates from the imaginary part of the finite-temperature dielectric function and, therefore, provides a direct measure of plasmon damping and lifetime within the RPA. In this sense, Γ plays a role analogous to the loss function $-Im\left[\varepsilon^{-1}(q,\omega,T)\right]$ commonly employed in spectroscopic studies of collective excitations. The pronounced enhancement of Γ near the gap-closure condition reflects the strong Landau damping induced by the expansion of the SPE continuum [3,17,21].

The plasmon-frequency maps in Figure 3 ($\triangle_{so} = 0.5E_F$) quantify how the perpendicular-field-induced sublattice asymmetry $\triangle_z$ reshapes the collective mode, complementing the dispersion plots in Figure 2. For both wave vectors ($qv_F = 0.3E_F$ *and* $qv_F = 0.5E_F$), the plasmon frequency decreases monotonically with increasing $\triangle_z$, reflecting the progressive reduction of the effective carrier stiffness as one valley-spin sector is driven toward a smaller bandgap. At $T = 0$, the softening is smooth across the entire $\triangle_z$ range, consistent with the upper panels and the lower right panel in Figure 2, in which, away from the gap-closure point, the plasmon remains largely outside the SPE continua, and Landau damping is weak. By contrast, at $T = 0$ *and* $T = 0.2T_F$, there is a pronounced drop near $\triangle_z \approx \triangle_{so}$, that is, where the gap-closure condition $\triangle_z \approx \triangle_{so}$ is satisfied. This is the regime shown in the lower left panel of Figure 2: the interband threshold collapses, the SPE region expands to lower energies, and the plasmon branch approaches (or enters) the continuum. Thermal broadening then enhances intra-/interband mixing, producing a sharper redshift and increased damping, which is more visible at the larger wave vector $qv_F =$

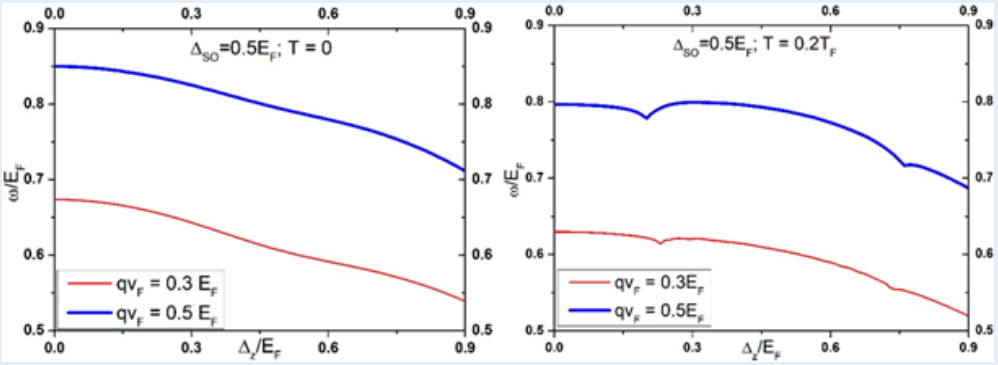

Figure 3: Plasmon frequency as functions of $\triangle_z$ at $\triangle_{so} = 0.5E_F$, $T = 0$ *and* $T = 0.2T_F$, plotted for several wave vectors.

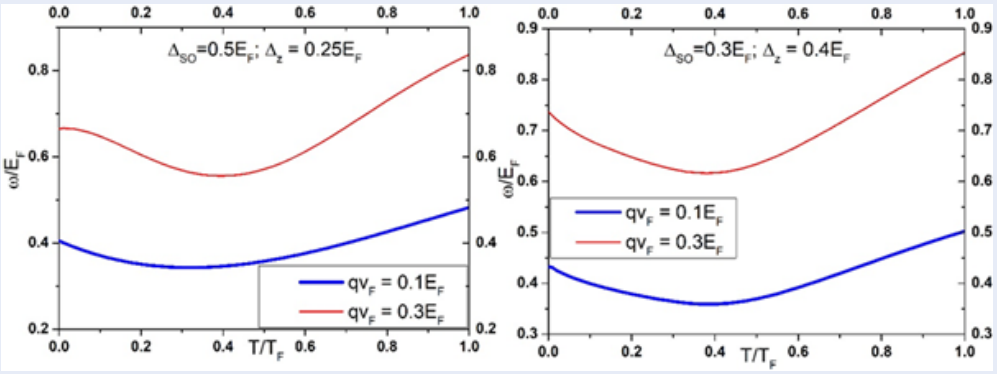

Figure 4: Variation of plasmon frequencies with temperature.

$0.5E_F$ because of its proximity to the SPE boundary. For $\triangle_z > \triangle_{so}$, the curves have a gentler slope, consistent with the "reopened gap" in the lower right panel of Figure 2, in which the undamped window is partially restored, and the temperature sensitivity decreases. Two robust trends can be seen in this set of results: (i) an increased temperature uniformly redshifts the plasmon's frequency and magnifies its sensitivity to $\triangle_z$, and (ii) the most vulnerable operating point occurs near $\triangle_z \approx \triangle_{so}$, where thermal effects and Landau damping combine to suppress the mode. Hence, stable device operation at a high temperature is favored in regimes with reopened gaps ($\triangle_z \neq \triangle_{so}$), particularly at smaller q.

Figure 4 presents the temperature dependence of the plasmon frequency w in MLS for two wave vectors ($qv_F = 0.3E_F$ *and* $qv_F = 0.5E_F$) under two representative mass configurations: (a) $\triangle_{so} = 0.5E_F$, $\triangle_z = 0.5E_F$, and (b) $\triangle_{so} = 0.3E_F$, $\triangle_z = 0.4E_F$. In both panels, the curves have a robust nonmonotonic behavior: starting from $T = 0$, ω first decreases with temperature, reaches a minimum at intermediate $T/T_F : 0.4 \div 0.6$, and then increases toward $T/T_F = 1$. The initial redshift originates from thermal broadening of the Fermi–Dirac distribution, which weakens the restoring force associated with intraband charge oscillations and enhances screening/damping. At higher temperatures, however, thermally activated carriers (including those from gapped spin-valley sectors) increase the intraband Drude weight and the real part of the finite T polarizability, producing a partial rehardening (blueshift) of the plasmon mode. The effect depends on the wave vector: the $qv_F = 0.3E_F$ branch lies at a higher absolute frequency and has a deeper minimum, consistent with its closer position to the SPE boundary in the dispersion maps. The parameter set (b), which is closer to the compensation condition $\triangle_z \approx \triangle_{so}$, shows a more pronounced high-T upturn than set (a), indicating that a near closure of one mass channel amplifies thermal activation and strengthens the recovery of the collective mode at high T. These trends are consistent with the four

dispersion plots: (i) a finite T generally redshifts and damps the plasmon, most strongly near gap closure; (ii) reopening the gap reduces thermal sensitivity; and (iii) a larger q enhances the temperature modulation. Overall, the data indicate that optimizing plasmonic operation at high T favors regimes away from $\triangle_z \approx \triangle_{so}$ and moderate q, where the mode remains well defined across the full temperature range.

It is important to note that temperature is expressed in terms of the reduced parameter T/T_F, which allows a direct mapping to different absolute temperature scales depending on the Fermi energy. As the temperature increases, the plasmon mode undergoes a gradual redshift and broadening due to enhanced thermal excitations and Landau damping, indicating a smooth crossover from weakly damped to more strongly damped collective modes [25,33].

CONCLUSIONS

We have systematically investigated finite-temperature plasmon excitations in MLS under electrically tunable sublattice asymmetry within the RPA framework. Our results demonstrate that temperature and external electric fields jointly control plasmon dispersion, damping, and stability. In particular, plasmon modes are most vulnerable near the gap-closure condition $\triangle_z = \triangle_{so}$, where the expansion of the single-particle excitation continuum leads to enhanced Landau damping. When the gap reopens, the undamped plasmon window is partially restored, improving mode stability. The observed nonmonotonic temperature dependence of the plasmon frequency reflects the competition between thermal broadening and thermally activated carriers. These findings provide guidance for designing thermally robust and electrically tunable plasmonic and optoelectronic devices based on silicene and related two-dimensional materials. Specifically, plasmon modes are most vulnerable near the gap-closure condition as a result of enhanced Landau damping, whereas operating in gap-reopened regimes improves their stability at finite temperature.

COMPETING INTERESTS

On behalf of all authors, the corresponding author states that there is no conflict of interest.

AUTHORS' CONTRIBUTIONS

Dong Thi Kim Phuong: Data analysis and manuscript drafting; Nguyen Van Men: Theoretical formulation, numerical programming, and manuscript revision.

ACKNOWLEDGEMENTS

This research is funded by Vietnam National University Ho Chi Minh City (VNU-HCM) under grant number B2025-16-01.

REFERENCES

1. AK G, KS N. The rise of graphene. Nature Mater. 2007;6(183).
2. J Z, H L, CC L, and Quhe R YZ, S Z, et al. Rise of silicene: A competitive 2D material. Progress in Materials Science. 2016;83(24).
3. CJ T, EJ N. Dynamical polarization function, plasmons, and screening in silicene and other buckled honeycomb lattices. Physical Review B. 2019;89(195410).
4. L S, CJ T, EJ N. Optical signatures of the tunable band gap and valley-spin coupling in silicene. . Physical Review B. 2012;86(195405).
5. M M, T V, fard T S, M F, B T. Plasmon-phonon coupling in a valley-spin-polarized two-dimensional electron system: a theoretical study on monolayer silicene. . Physical Review B. 2018;98(045429).
6. A A, MS V, L V, A C, A P. Plasmonics with two-dimensional semiconductors: from basic research to technological applications. . Nanoscale. 2018;10(8938).
7. Physics and Applications of Graphene – Theory. InTech, Janeza Trdine 9. 2011;.
8. SA M. Plasmonics – Fundamentals and Applications . Springer. 2007;.
9. X L, T Q, and Ni Z LW. Plasmons in graphene: Recent progress and applications. Materials Science and Engineering: R: Reports. 2013;74(351).
10. M J, M S, H B. Plasmons in Graphene: Fundamental Properties and Potential Applications. . In: Proceedings of the IEEE; 2013.
11. D E, A P, S J. Photothermal response of plasmonic nanofillers for membrane distillation. . The Journal of Chemical Physics. 2020;152(114102).
12. D S, V R, V V, T O. Voltage-controlled surface plasmon-polaritons in double graphene layer structures. . J Appl Phys. 2013;113(053701).
13. D S, T O, and Ryzhii V DZ. Plasmons in tunnel-coupled graphene layers: Backward waves with quantum cascade gain. Physical Review B. 2016;94(115301).
14. P P, TJ C. Dynamical polarization and plasmons in a two-dimensional system with merging Dirac points. . Physical Review B. 2016;93(8):085145.
15. CJ T, EJ N. Magneto-optical conductivity of silicene and other buckled honeycomb lattices. . Physical Review B. 2013;88(085434).
16. H-R C, J Z, H Z, Y Y. Probing the topological phase transition via density oscillations in silicene and germanene. . Physical Review B. 2014;89(201411(R)).
17. Iurov A, Gumbs G, Huang D. Temperature-dependent collective effects for silicene and germanene. . Journal of Physics: Condense Matter. 2017;29(135602).
18. NV M, DTK P. Silicene-2DEG heterostructures: Collective excitations investigations. . Physica B. 2023;668(415257).
19. NV M. Plasmon modes in N-layer silicene structures. . Journal Of Physics-Condensed Matter. 2022;38(4):085301.
20. CV G, M P, M G, P R, A S. Plasmon properties and hybridization effects in Silicene. . Physical Review B. 2017;95(085419).
21. N D, T V, M F, fard T S. A theoretical study of collective plasmonic excitations in double-layer silicene at finite temperature. . Journal of Applied Physics. 2019;125(104302).
22. NV M, DTK P. Temperature effects on plasmon modes in double-bilayer graphene structures. . Solid State Communications. 2021;334-335(114398).
23. NV M, DTK P. Plasmon modes in double-layer gapped graphene at zero temperature. . Physics Letters A. 2020;384(126221).
24. T V, T A, M F, F P. Temperature effect on plasmon dispersions in double-layer graphene systems. . Physics Letters A. 2010;374(48):4899.

25. DK P, SSZ A, AC S. Temperature dependent screened electronic transport in gapped graphene. . Physica Status Solidi B. 2015;252(8):1817.
26. JY W, SC C, MF L. Temperature-dependent Coulomb excitations in silicene. . New Journal of Physics. 2014;16(125002).
27. JY W, SC C, MF L. Plasmon modes in MLG-2DEG heterostructures: Temperature effects. . Physics Letters A. 2019;183(1364).
28. J-J Z, SM B, FM P. Plasmonic excitations in Coulomb-coupled N-layer graphene structures. . Physical Review B. 2013;87(085401).
29. NV M, NQ K. Plasmon modes in Dirac–Schrödinger hybrid electron systems including layer-thickness and exchange-correlation effects. Can J Phys. 2018;96(915).
30. DV T, NQ K. Plasmon modes of double-layer graphene at finite temperature. . Physica E. 2013;54(267).
31. NV M, DTK P. Plasmon modes in graphene GaAs heterostructures at finite temperature. . Int J Mod Phys B. 2019;33(16):1950174.
32. NV M, NQ K, DTK P. Plasmon modes in double bilayer graphene heterostructures. . Solid State Communications. 2013;294(43).
33. M R, M V, R A, M P, AH M. Finite-temperature screening and the specific heat of doped graphene sheets. . Journal of Physics A: Mathematical Theoretical. 2009;42(21):214015.
34. NV M. Temperature and inhomogeneity combination effects on collective excitations in three-layer graphene structures. . Physica E. 2022;140(115201).